**University of Naples "Federico II"**


*PhD Programme: "Industrial Product and Process Engineering"*

*XXIX Cycle*

# *DESIGN OF 3D VIRTUAL AND ADDITIVE MANUFCTURED MODELS FOR CULTURAL HERITAGE*

**Author:**
*Francesco Colella*

**Tutor:**
*Prof. Antonio Gloria*
*Prof. Massimo Martorelli*

**Coordinator:**
*Prof. Giuseppe Mensitieri*

# *Table of Content*

# Chapter 1
# Additive Manufacturing and Basic Concepts

## 1.1 INTRODUCTION

The ASTM International Committee F42 on AM technologies defines AM as the "process of joining materials to make objects from three-dimensional (3D) model data, usually layer by layer, as opposed to subtractive manufacturing methodologies (ASTM F2792–10 Standard Terminology for Additive Manufacturing, 2009,).

Generally, AM technologies involve the use of a computer, 3D modelling software (CAD), machine equipment and specific materials.

Once a CAD model is produced, the model data, usually converted in stereolithography (STL) format, are first decomposed into a series of 2D, finitely thick cross sections, which are then fed into an AM machine that lays downs or adds successive layers of liquid, powder, sheet material or other, in a layer-upon-layer fashion to fabricate a 3D object metals, ceramics, polymers, composites, or biological materials.

If compared to o traditional technologies, AM processes have many advantages such as a cost-effective and time-efficient way to produce low-volume, customized products with complex geometries and improved properties/functionality (Staiano, 2016).

From the first patent registered on March 11, 1986 from Charles W. Hull, up to the present day, AM has evolved into a different kinds of processes, including Stereolithography (SLA), Fused Deposition Modeling (FDM), Laminated Object Manufacturing (LOM), Selective Laser Sintering

(SLS), Selective Laser Melting (SLM), Direct Metal Deposition (DMD), Laser Metal Deposition (LMD), inkjet printing, and others.

It is well known that reverse engineering and additive manufacturing may be suitably integrated to develop different kinds of customized devices. Starting from image capture and analysis techniques, it is possible to manufacture an object or a functional part in a layer-by-layer fashion. Today many objects may be fabricated by additive manufacturing, benefiting from user-friendly computer programs and from the availability of open source 3-D printers.

In the field of cultural heritage, there are many potential applications of the reverse engineering tools and methods, ranging from dissemination (e.g., virtual museums), reproduction (e.g., via additive manufacturing) and maintenance, to condition monitoring.

Accordingly, in the proposed research 3D virtual and physical scale models of buildings and artworks were properly developed.

3D physical models were fabricated by fused deposition modeling (FDM), starting from the optimization of the process and instrument parameters.

The processability of the materials (i.e., thermoplastic polymers) was assessed through functional and calorimetric analyses. Image capture and analysis techniques allowed to reproduce the geometry and morphology.

Among the different AM technologies currently available, in the present study Fusion Deposition Modeling (FDM) was considered to manufacture 3D physical models for cultural heritage (i.e., buildings, artworks) using thermoplastic polymers.

To optimize the manufacturing conditions, some concepts related to the process parameters and materials were taken into account.

## 1.2 Additive Manufacturing Processes

AM processes include countless technologies that fabricate three-dimensional parts layer upon layer starting from a CAD model.

AM processes can be categorized following two different criteria [8]: the first one is based on the kind of technology used, while the second one is based on the kind of material that can be processed (Staiano, 2016).

With respect to the physical state of raw material, AM processes are classified into four principal classes, based, respectively, on liquid, filament/paste, powder or solid sheet.

AM processes may also be classified depending on the class of raw materials, such as polymers, metals, ceramics, composites and biological materials (Staiano, 2016).

According to ASTM F42 Committee AM processes were classified into seven categories shown in Table 1.

| Process Category | Technology | Part Material |
|---|---|---|
| Vat photopolymerisation | SLA | UV curable resins<br>Waxes<br>Ceramics |
| Material jetting | MJM | UV curable resins<br>Waxes |
| Binder jetting | 3DP | Polymer<br>Metal<br>Composites |
| Material extrusion | FDM | Thermoplastic<br>Waxes |
| Sheet lamination | LOM | Paper<br>Metal<br>Thermoplastic |
| | UAM | Metal |
| Directed energy deposition | LMD | Metal |
| | LENS | Metal |
| Powder bed fusion | SLS | Thermoplastic<br>Metal |
| | DMLS | Metal |
| | SLM | Metal |
| | EBM | Metal |
| | SHS | Thermoplastic |

*Table 1: AM Processes categories*

An overview on different AM categories and their main characteristic, is described [8].

- Vat photopolymerisation (Stereolithography, SLA) uses a vat of liquid photopolymer resin, out of which the model is constructed layer by layer using an ultraviolet (UV) light to harden the resin, where required, whilst a platform moves the object being made downwards after each new layer is polymerized.
- Material jetting (Multi Jet Modeling, MJM) jetting material onto a build platform, using a Drop On Demand (DOD) approach, where it solidifies and the model is built layer by layer.

Material is deposited from a nozzle which moves horizontally across the build platform in a similar method to a two dimensional ink jet printer.

The material layers are then polymerized using ultraviolet (UV) light.

- Binder jetting (3D Printing, 3DP) involves building a model in a container filled were, for each layer, a roller spreads and compress a measured amount of material powder, such as either starch or plaster material, over the building platform.

  For each layer, a multichannel jetting head applies a calibrated quantity of liquid adhesive to bond the particles of material together and form the two-dimensional cross section of the object (Staiano, 2016).

  Upon application of the binder, a new layer is swept over the prior one, with the application of more binder, and this process is repeated until the model is complete.
- Material extrusion (Fusion Deposition Modeling, FDM) involves feeding a thermoplastic filament (typical thickness 1.75÷3 mm) into a heated extrusion nozzle that melts and deposits the material moving, by convention, in the X and Y axes, to form the horizontal plane on a table that moves, on the Z axis, to build up layer by layer the model.
- Sheet lamination processes include Laminated Object Manufacturing (LOM) and Ultrasonic Additive Manufacturing (UAM).
  - LOM use paper material and adhesive, basing on a layer by layer approach and, for this reason, are often used for aesthetic and visual models and are not suitable for structural use.

    The process uses a cross hatching method, during the printing process, to allow for easy removal post build.
  - UAM process uses sheets, or ribbons, of metal, which are bound together by ultrasonic welding involving low temperature and allowing to create internal geometries.

The UAM requires, often during the welding process, additional CNC (Computer Numerical Control) machining and removal of the unbound metal. As the metal is not melted, the process requires relatively low energy and different materials can be bonded.

- Directed Energy Deposition (DED), that includes Laser Metal Deposition (LMD) and Laser Engineered Net Shaping (LENS) processes, is a more complex printing process commonly used to repair or add additional material to existing components.

  Typically machine, consists of a nozzle mounted on a multi axis arm, which deposits melted material onto the specified surface, where it solidifies.

  The principle of process is similar to material extrusion, but, otherwise, the nozzle is not fixed to a specific axis and can move in multiple directions.

  The material, which can be deposited from any angle due to 4 and 5 axis machines, is melted upon deposition with a laser or electron beam. The process is typically used with metals but polymers and ceramics can be used in the form of either powder or wire.

  - Laser Metal Deposition (LMD) built up the part, layer by layer, using a laser beam to form a melt pool on a metallic substrate, into which powder is fed from a nozzle.

    The powder melts to form a deposit that is bonded to the substrate and both the laser and nozzle are manipulated using a gantry system or robotic arm.

  - Laser Engineered Net Shaping (LENS) fabricates three-dimensional metal component deposing, sequentially, consecutive layers using a metal powder injected into a molten pool created by a focused, high-powered laser beam.

    Simultaneously, the substrate on which the deposition is occurring is scanned under the beam/powder interaction zone to fabricate the desired cross-sectional geometry.

- Powder Bed Fusion processes include the following printing techniques: Direct Metal Laser Sintering (DMLS), Electron Beam Melting (EBM), Selective Heat Sintering (SHS), Selective Laser Melting (SLM) and Selective Laser Sintering (SLS).

The fundamental difference between these technologies is the mean that they use to expose the powder (electron beam, laser beam or thermal print-head).

- Direct Metal Laser Sintering (DMLS) is the same layer by layer process as Selective Laser Sintering (SLS) but the first one sintering metals materials, while, the second one sintering polymeric materials.
- Electron Beam Melting (EBM), usually used to build functional parts in metals and alloys materials, require a vacuum ambient. All powder bed based processes involve the spreading of the powder material over previous layers, by means of different mechanisms, including a roller or a blade.

  A hopper or a reservoir below of aside the bed provides fresh material supply.
- In Selective Heat Sintering (SHS), layers are added with a roller in between fusion of layers and the platform lowers the model accordingly but differs from other processes, since it uses a heated thermal print head to fuse powder material together.

## 1.3 Fused Deposition Modeling (FDM)

Based on previous works [9], [10] and [11], the analysis and the optimal setup of the printing process parameters, for FDM process have been identified using a DOE approach.

Until a few years ago, manufacturing high-quality physical prototypes or products required very expensive AM systems and investments in tooling and sophisticated specific software. This posed a barrier to the widespread deployment of such systems, now used by big companies, research institutes or innovative start-ups (Staiano, 2016).

3DP is rapidly becoming available to the masses thanks to recent developments driving down the cost and complexity of the machines.

The current expansion of the new generation 3D printers has benefited from the expired 3DP patents for fused deposition modeling, where objects are built up layer by layer with extruded polymer) and from the open-source movement (for both software and hardware—Arduino hardware).

Available on the web, the cost of these new open-source 3D printers ranges from 400 to 2000 €.

Today, new low-cost AM systems allow for the production of parts also in metal [12], [13] and [14].

3DP is considered as the production technology of the future, enabling "the third industrial revolution" [15], [16] and [17].

In recent times, the increasing interest of industry in RP processes and their application is also evident from the development of standards through ASTM International and the International Organization for Standardization (ISO) [18] and [19].

One of the most famous and successful open-source projects of 3D printer development is known as the RepRap (replicating rapid prototyper) Project [20].

It was developed in 2005 by Adrian Bowyer with the University of Bath (UK).

The aim was to develop a 3D printer capable of replicating a significant number of its own structural components.

The remaining parts were selected from standard engineering materials and components available cheaply worldwide. This project is original and unique.

Currently, for these systems there is a significant lack of scientific data concerning the appropriate selection of process parameters in order to improve accuracy and to save time. In a previous study, an open-source RepRap Prusa-Mendel I2 3D printer (0.35mm nozzle diameter) and a 2.85mm PLA biodegradable material were used with the aim to evaluate the impact on system accuracy of important process parameters such as layer thickness, deposition speed, and flow-rate, as well as to improve the knowledge about optimal settings. First, the 3D printer was calibrated. The calibration phase of a RepRap 3D printers, in fact, is a fundamental phase. It allows the motors to move the correct distance each time they move the build platform or the extruder, so as to obtain objects with the same dimensional characteristics, also if they are fabricated by different RepRap of the same type (for this research Prusa-Mendel I2).

The calibration was performed using a dial indicator with magnetic base, Mitutoyo 2046-08 (Mitutoyo, Japan) with an accuracy of ±µm. MARLIN (open-source) was used as the firmware software and CURA (open-source) as the software which converts STL files into G-code files able to command and control the system in order to obtain the final 3D object printed.

The methodology employed in this study consists of sequential procedures aimed to produce and measure benchmarking parts made using the RepRap Prusa-Mendel I2. Figure 1 shows the general work flow adopted.

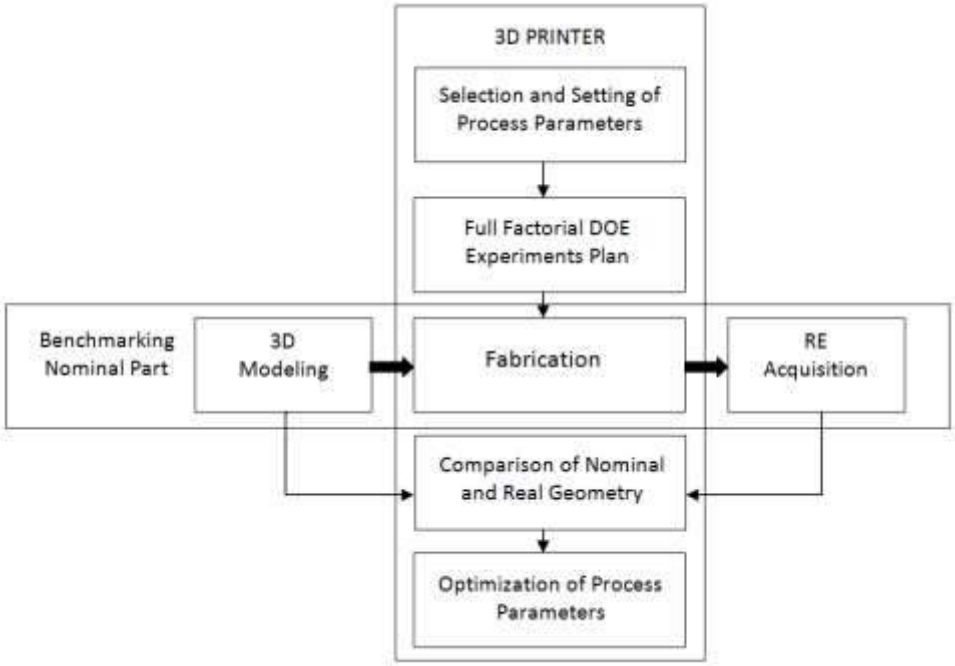


*Figure 1: Logical work-flow for the comparison of benchmarking nominal and real parts fabricated following a full factorial design.*

Various studies on the design of benchmarking parts for evaluating the accuracy and repeatability of RP processes are available, see for example, Kruth [21], Lart [22], Iuliano et al. [23], Juster and Childs [24] and [25], Shellabear [26], Mahesh et al. [27], and Hopkinson and Sercombe [28].

Unfortunately, however, none of the proposed parts comprehensively included all the features necessary to establish the desired accuracy/repeatability related parameters.

In 2012, Fahad and Hopkinson [29] proposed a new benchmarking part (Figure 2 on the left) that includes elementary shapes representative of all the main features useful for evaluating accuracy and repeatability (cube, cylindrical hole, sphere, solid cylinder, hollow cylinder, cone, angled surfaces) in a very compact manner.

Ten features are replicated three times to evaluate variability.

This benchmarking part was taken into account for this study but to allow the fabrication in the same printing and laser scanner acquisition, the 10 features were placed side by side as shown in Figure 2 on the right.

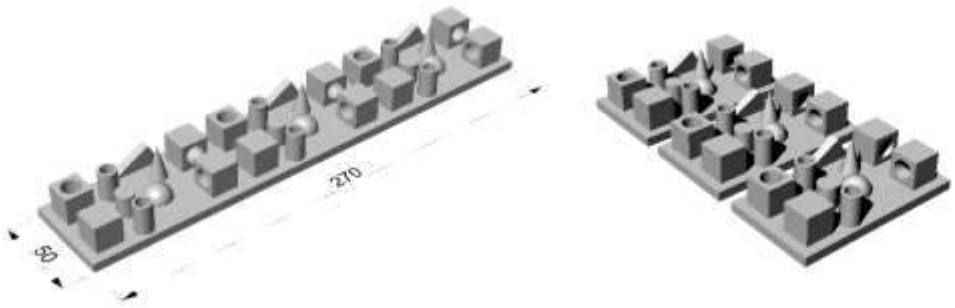


*Figure 2: Benchmarking part [29] with three replications of 10 main features used in the study,*

The study of the factors involved in the experimentation is a crucial task.

It was done mainly through focus group with RepRap experts and on the basis of literature review related to consolidated RP processes.

Layer thickness (A), deposition speed (B), and flow rate (C) were adopted as control factors. Table 2 shows other process parameters that were held constant throughout the experimentation.

The control factors can be set in all the main slicing software (CURA, KISSLICER, SLIC3R, SIMPLIFY3D) and they are defined as:

- Layer thickness (mm) is the thickness of each slice of the part building and it is the step along the vertical axis taken before extruding a new layer atop the previous one. In Refs. [30] and [31], it is known that with a lower layer height a better accuracy of the part is obtained.
- Deposition speed (mm/s) is the speed with which the hotend moves; with a lower deposition speed it is obtained a better accuracy of the part but an increase in the fabrication time.
- Flow rate (%) is the flow of material that is extruded from the hotend and is expressed as a percentage of the number of revolutions that the motor of the extruder has to do, to extrude 1mm of filament.

| ***Constant factors*** | ***Value*** |
|---|---|
| *Wall thickness (mm)* | *0.7* |
| *Bottom/top thickness (mm)* | *0.6* |
| *Fill density (%)* | *20* |
| *Bed temperature (°C)* | *80* |
| *Printing temperature (°C)* | *200* |

*Table 2: Process parameters held constant throughout the experimentation*

For each control factor, the range of variation was chosen considering that the aim of the study is to understand the main effects of process parameters on the accuracy.

For the layer thickness, considering that with a lower deposition speed it is obtained a better accuracy of the part, as mentioned above, the authors, in the predesign phase, carried out tests with a layer thickness value of 0.05 mm.

Therefore, for the layer thickness the minimum value chosen was 0.10 and it was increased in steps of 0.05 mm.

For the deposition speed, the range of typical values is 30–120 mm/s. Considering that with a lower deposition speed it is obtained a better accuracy of the part, as mentioned above, the authors, to ensure the best performance in term of accuracy, considered the minimum value of 30 mm/s and a maximum value of 80 mm/s.

For the flow rate, based on the experience of the RepRap experts the three values, 100%, 105%, and 110% were chosen.

All control factors and conditions set for the experimental treatments are listed in Table 3.

| ***Factor*** | ***Level*** | | |
|---|---|---|---|
| | *-1* | *0* | *1* |
| *A - Layer thickness (mm)* | *0.10* | *0.15* | *20* |
| *B - Deposition speed (mm/s)* | *30* | *55* | *80* |
| *C - Flow rate %* | *100* | *105* | *110* |

*Table 3: Control factors and their levels for the fabrication of the benchmarking parts*

A full factorial design, with three factors at three levels (see ANNEX II), and three replications (Figure 2) was carried out to obtain 81 PLA prototype using Prusa-Mendel I2 [32], [33] and [34]. Each benchmarking part was acquired using a high resolution Laser Scanner, D700 Scanner—3Shape, Denmark to generate the cloud points.

The accuracy of this noncontact Reverse Engineering system is of ±20μm.

RE acquisition should be defined a noise factor adding a variation to the process.

For this study it has been considered as a constant factor, because all the parts are acquired by the same laser scanner and operator following the same procedure.

In this way the variation due to the acquisition is effectively smaller than variation due to process.

The 3D models obtained were then compared with the nominal CAD model, i.e., nominal benchmarking part.

Data processing was performed in GEOMAGIC software, using an iterative closest point algorithm [35], to minimize the distance between the clouds point and nominal CAD model. The choice of alignment between point cloud and nominal CAD model should be a noise factor.

In this exploration study it has been considered as a constant factor, because all parts were aligned using the same procedure and the point clouds were checked by the same expert operator.

Two planes and one sphere were used to fit each point cloud to CAD model.

The YZ plane was obtained selecting two aligned sides of external cubes, the XY plane was obtained selecting the upper surface of the base and the sphere was obtained selecting the hemisphere.

These data allow to define the alignment procedure of each point cloud and the CAD model: two data plane lock five degree of freedom and the last one is locked by the datum sphere (Figure 3).

All sequences of three data (sphere, XY plane, and YZ plane) were evaluated to choose the optimal alignment (Staiano, 2016).

In order to minimize deviation, the adopted alignment sequence was sphere - XY plane - YZ plane.

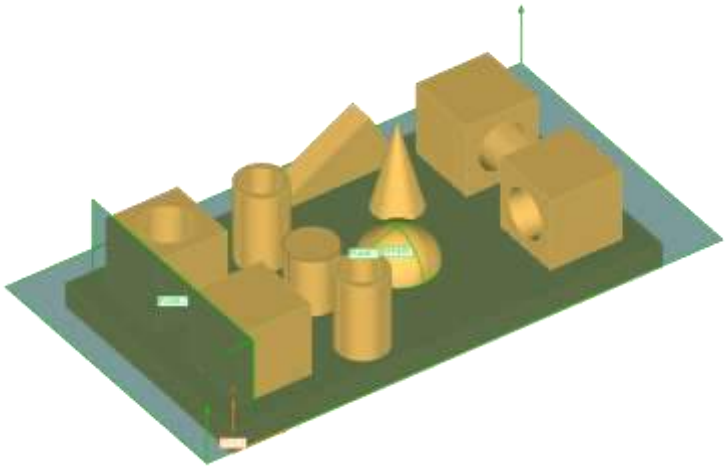

*Figure 3: Alignment of the point clouds with the CAD model through the three datum*

Starting from the results reported in ANNEX II, it can be highlighted that:

- Factor B is the most important factor with a CR equal to 34%.
- Factors A and C are equally important having the same CR equal to 22%.
- Interactions AC and AB show a cumulated CR equal to 16%, so it should be useful to take into account the simultaneous effect of both interactions even if each interaction seems to be not significant.
- Cumulated CR of factors A, B, C, AC, and AB is greater than 90% that is the Pareto ANOVA threshold [32] to take into account significant effects.

The main effect plot (Figure 4) shows that the choice of the levels -1 of factor A (0.10 mm), -1 of factor B (30 mm/s), and 0 of factor C (105%), is the optimal expected combination that maximizes the accuracy, i.e., minimizes RMS.

The interaction plots (Figure 5) show that the choice of the level -1 of factor A (0.10 mm) mitigates the accuracy loss when factor B is selected at level 0 (30 mm/s) .

Furthermore, the same effect happens when factor A is at level -1 (0.10 mm) or level 0 (0.15 mm) and the factor C is selected at level 0 (105%) or level 1 (110%).

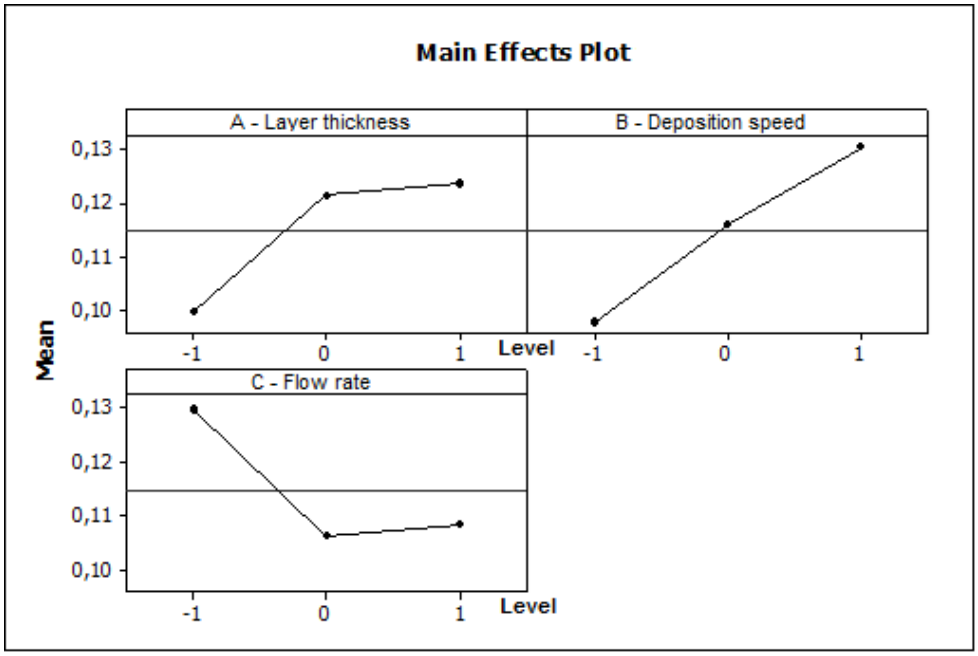


*Figure 4: Main effects plot of the three process parameters (A,B,C) at three levels (-1,0,1) on the response RMS*

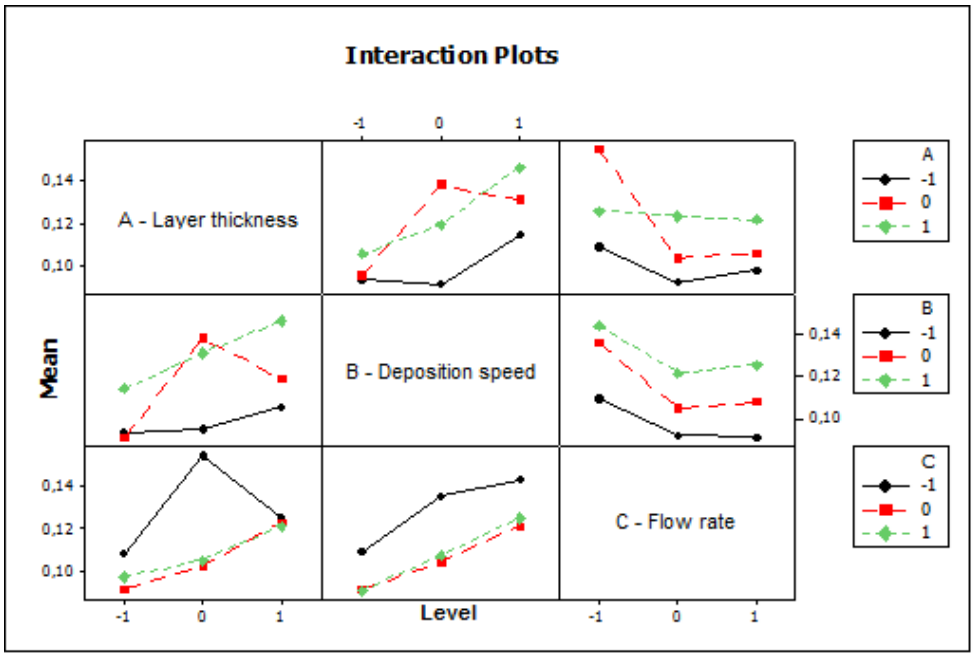


*Figure 5: Interaction plots of the three process parameters (A,B,C) at three levels (-1,0,1)on the response RMS*

It also can be settled out that:

- The lowest value of deposition speed (factor B), i.e., 30 mm/s, maximizes the accuracy. The expected result is in accordance with common sense.
- The lowest value of layer thickness (factor A), i.e., 0.10 mm, maximizes the accuracy. This value can be considered as an optimal value because previous tests, carried out considering layer thickness values less than 0.10mm (e.g., 0.05 mm), showed accuracy loss of the prototype.

  This result agrees with a "rule of thumb" that empirically suggest a value of layer thickness equal to one-fourth of the nozzle as optimal choice (in this test the diameter is 0.35 mm).
- The choice of level 1 (110%) is acceptable being the RMS differences very small if compared to the results of level 0. So the practical suggestion to increase the flow rate over the 100% is correct and the effects on the accuracy are robust, being the improvement obtained in a wide range (from 105% to 110%).

- The best prototype was n. 2. This result agrees with the expected optimal combination (-1,-1,0) and it suggests that the mean effect model well fits real data.
- The worst prototype was n. 13. It was obtained with the combination (0,0,-1).

  This result highlights a significant effect of interaction. It means that the mean effect model (i.e., the model without interactions) does not explain completely real data. This limit requires new experimental tests to improve model fitting and to better understand the interactions as source of variability.

Starting from these results, to give new practical insight about the choice of process parameters, the fabrication time is taken into account (Staiano, 2016).

Table 4 shows the best and worst prototypes in terms of accuracy and fabrication time and some good compromise in terms of both responses.

The first practical suggestion is that maximum accuracy is not correlated to maximum fabrication time, being significant the effect of flow rate.

The second practical suggestion is that to save time, the layer thickness can be increased to the highest value. In this case, the time saving is about 50% and the loss in accuracy is approximately 25%.

The third practical suggestion is that if the accuracy is not critical (being acceptable till a mean value of 0.15) it is recommended to set both layer thickness and deposition speed to the highest value to obtain the minimum fabrication time.

In this case the interaction effect is meaningful, being this setting robust against flow rate variation.

| Prototype | Factor | | | Mean rms [mm] | St.dev. | Time [min] |
|---|---|---|---|---|---|---|
| | A | B | C | | | |
| 2 | -1 | -1 | 0 | 0.08 | 0.011 | 288 |
| 3 | -1 | -1 | 1 | 0.09 | 0.003 | 288 |
| 21 | 1 | -1 | 1 | 0.10 | 0.004 | 148 |
| 20 | 1 | -1 | 0 | 0.10 | 0.005 | 148 |
| 14 | 0 | 0 | 0 | 0.10 | 0.002 | 160 |
| 4 | -1 | 0 | -1 | 0.10 | 0.010 | 229 |
| 1 | -1 | -1 | -1 | 0.11 | 0.015 | 288 |
| 26 | 1 | 1 | 0 | 0.14 | 0.005 | 115 |
| 27 | 1 | 1 | 1 | 0.15 | 0.010 | 115 |
| 25 | 1 | 1 | -1 | 0.15 | 0.011 | 115 |
| 13 | 0 | 0 | -1 | 0.20 | 0.072 | 160 |

*Table 4: Control factors and their levels for the fabrication of the benchmarking parts*

The final suggestion is to take care of level settings and to avoid neutral choice.

## 1.4 Direct Metal Laser Sintering (DMLS)

Direct Metal Laser Sintering (DMLS) is a typical Additive Manufacturing (AM) process based on the layer by layer powder spreading and subsequent laser sintering [36].

Therefore, DMLS enables production of complex 3D shaped functional parts directly from metal powders.

Based on the experience of experts and on literature review, a number of variables introduced by the DMLS process, such as laser scan speed, layer thickness, support structures, and part orientation that contribute to the final geometric tolerances and surface roughness and that affect the final quality of the part, have been taken into account (Staiano, 2016).

The main causes of variability in the DMLS process and the relative impact in the final characteristics of the printed part, are reported and grouped in respect of raw materials, of model data preparation and setup of printing process in the Table 5, Table 6 and Table 7.

Materials behave differently during the sintering/melting process so it is necessary to customize exposure, recoating, and heating settings for each raw powder.

Obviously, within the same kind of raw material, properties of the individual powder batch that is loaded into the printer, have an effect on working conditions, energy input, part throughput and post-processing.

Anomalous values of these properties could generate variability within sintering/melting operations, hence in the final characteristics of the printed part.

Material properties that could enhance DMLS process variability are resumed in the Table 5, together with their common effects [37].

| ***Material property*** | ***Material property*** |
|---|---|
| *Particle size distribution* | *Sinterability/meltability*<br>*Packing efficiency*<br>*Surface roughness* |
| *Particle shape* | *Packing efficiency* |
| *Apparent / tap density* | *Packing efficiency* |
| *Melting point* | *Indicator of energy requirements* |
| *Strength of green part* | *Facilitates part handling before thermal cycle (debinding, sintering, infiltration)* |
| *Specific heat, thermal conductivity* | *Heat transfer in powder bed* |
| *Void fraction* | *Residual porosity in printed parts* |
| *Flowability* | *Uniform spreading of powder layer* |

*Table 5: Sources of variability in DMLS processes due to the properties of materials*

An appropriate data preparation is an important prerequisite for the correct implementation of ALM processes and to avoid a job failure or the poor quality of the produced parts.

Some of countless geometric and topological parameters that affect this phase are presented in Table 6.

| ***Geometric / topological parameter*** | ***Affected characteristic*** |
|---|---|
| *Part inclination (build angle)* | *Mechanical properties*<br>*Part accuracy*<br>*Process speed* |
| *Part positioning on the plate* | *Mechanical properties*<br>*Part accuracy*<br>*Shrinkage/distortion* |
| *Part orientation* | *Mechanical properties*<br>*Part accuracy*<br>*Shrinkage/distortion* |
| *Type and number of supports* | *Mechanical properties*<br>*Process speed*<br>*Wasted material amount*<br>*Surface roughness* |
| *Z- height* | *Process speed*<br>*Part accuracy*<br>*Surface roughness* |
| *Layer thickness* | *Mechanical properties*<br>*Part accuracy*<br>*Process speed* |

*Table 6: AM process variability due to geometrical and topological settings*

Layer thickness has a fundamental role in respect to the process speed and part accuracy.

Generally, low levels of layer thickness result in better geometrical and mechanical properties of the sintered part.

However, a small layer thickness always involves increased build times.

In DMLS process, every protruding, or overhanging, surface needs to be fixed on the building platform and properly supported, in order to allow the layer-by-layer growth of the part. This is

achieved by means of fixation structures, called supports. Supports require time and material to be created (as well as the part).

Moreover, after building they have to be removed from the platform and the part by sawing, wire-cutting or spark-erosion.

Before choosing the supporting strategy, it is important to analyse the part orientation and inclination according to specific criteria such as:

- z-height - larger z-height can reduce the amount of surfaces which have to be supported, but it increases build time and risk of supports collapse;
- maximum cross section – minimizing the exposure area per layer ensures the heat drain from exposure areas and reduces the internal stress, thus enhancing mechanical properties;
- growing direction – as well as for the part, preventing the growth of supports to run counter the powder spreading direction, results in reduced risk of lifting of a layer under the action of the re-coating blade, which can cause distortion and irregularities within the processed material, damage to the blade itself and interruption of printing process.
- build angle – Higher build angles lead to increased build times, but they are necessary to reduce internal stresses and improve part quality for some geometries.

When the part has been oriented, the operator can proceed to generate support structures, bearing in mind the countless critical issues in executing this step, such as removability, surface quality alteration and heat drain from the part.

The positioning on the building area also affects the final properties of parts, depending on the print volume isotropy characteristics of the used device.

During printing (sintering/melting) phase, variability can arise mainly to ambient conditions and exposure settings such as laser power, (that affects the amount of energy that can be delivered to the material) or hatching distance (that is the distance between the lines during the sintering of inner

area, after the contour exposure, that affect the mechanical strength and also surface roughness of the DMLS prototypes).

Compliance with the ambient conditions is essential for a trouble-free process and for avoiding wear or degradation of the equipment, as shown in Table 7.

| ***Geometric / topological parameter*** | ***Affected characteristic*** |
|---|---|
| *High temperature in room* | *Overload of the cooling system*<br>*Inadequate cooling of the optical assemblies*<br>*Formation of condensed water on cooled assemblies* |
| *Low temperature in room* | *Formation of condensed water on trim panels and housings* |
| *High ambient moisture content in room* | *Formation of condensed water on trim panels and housings* |
| *Inadequate supply of inert gas* | *Building process is interrupted* |

*Table 7: Sources of variability in AM processes due to ambient conditions*

Open literature, focuses on the fundamentals of the laser sintering process and the evaluation of the materials produced by this method by looking at mechanical properties and microstructure have investigated the application of DMLS to actual component quality.

Some of these studies have quantified the surface roughness and the effect of process variables on the final part quality.

Simchi et al. [38] studied a simple iron-based DMLS part and reported surface roughness while Khaing et al. [39] reported roughness for a nickel–bronze–copper DMLS part evaluating, in addition the geometric tolerance of the test specimen.

Senthilkumaran et al. [40] and Song and Koenig [41] investigated the effect of various DMLS process parameters (laser scan speed, laser power, and hatching distance) on the surface roughness.

Delgado et al. [42] studied, in addition, the effect of build direction on surface roughness and dimensional tolerance for stainless steel DMLS parts.

Wong et al. [43] examine heat transfer and pressure loss through additively manufactured heat exchangers.

Calignano et al. [44] investigated the effect of various DMLS process parameters studying DMLS of AlSi10Mg powder through an experiment based on Taguchi approach in order to assess the influence of processing parameters (hatching distance, scan speed and laser power) on surface roughness.

It obtains that low scan speeds resulted to improve the top surface finish giving to the melt pools more time to flatten before solidification.

On the other side, a too low scan speed could increase the volume of liquid produced within the melt pool and balling phenomenon could arise.

With respect to laser power, higher values resulted in reducing the melt pool tendency to undergo balling by relieving surface tension variations.

However, if laser power is too high, material vaporization can occur and recoil pressures can disrupt the melt pool surface.

N. Read, et al. [45] investigate the influence of Selective Laser Melting (SLM) process parameters on the porosity development in AlSi10Mg was investigated by means of DOE approach, focusing on laser power, scan speed, scan spacing and island size. Experimenters identified a low energy density region corresponding to a high porosity due to the lack of consolidation and a high energy

density region (approximately over 60 J/mm$^3$) where other defects, such as keyhole formation (due to vaporization), have been observed within the material.

These information allow to evaluate and optimize the correct DMLS printing process conditions.

However, differently from Read et al., a new additive manufacturing processes was used to develop system with improved properties [46] (Staiano, 2016).

# Chapter 2
# Materials Analysis and Fabrication Methods

## 2.1 Materials and Manufacturing

3D virtual and physical models for cultural heritage were designed and manufactured by reverse engineering approach and fused deposition modeling (FDM) using two Acrylonitrile-Butadiene-Styrene (ABS)-based thermoplastic polymers and a 3D printer (Zortrax S.A, Poland).

Two thermoplastic polymers (under the trade name Z-ABS and Z-UltraT) were selected in the form of filaments with a diameter of 1.75.

Some mechanical properties related to the Z-ABS material [47] Z-UltraT [47, 48] are reported in Table 2.1 and Table 2.2.

| ***Mechanical Properties*** | ***Test Method*** | ***Value*** |
|---|---|---|
| *Young's Modulus* | *DIN EN ISO 527-2 (ASTM D638)* | *1.80 GPa* |
| *Tensile Strength* | *DIN EN ISO 527-2 (ASTM D638)* | *38 MPa* |
| *Tensile elongation* | *DIN EN ISO 527-2 (ASTM D638)* | *17 %* |
| *Rockwell R hardness* | *PN-EN ISO 2039-1 (ASTM D785)* | *109* |

*Table 2.1. Mechanical properties of Z-ABS.*

| *Mechanical Properties* | *Test Method* | *Value* |
|---|---|---|
| *Young's Modulus* | *DIN EN ISO 527-2 (ASTM D638)* | *1.95 GPa* |
| *Tensile Strength* | *DIN EN ISO 527-2 (ASTM D638)* | *42 MPa* |
| *Tensile elongation* | *DIN EN ISO 527-2 (ASTM D638)* | *21 %* |
| *Rockwell R hardness* | *PN-EN ISO 2039-1 (ASTM D785)* | *110* |

*Table 2.2. Mechanical properties of Z-UltraT.*

## 2.2 Calorimetric analysis

Differential Scanning Calorimetry (DSC) and thermogravimetric analysis (TGA) were performed on Z-ABS and UltraT at 10°C/min, according to the ASTM D3417 [49] and ASTM D3418 [50].

Such test method covers the determination of heat of fusion and heat of crystallization of polymers by DSC.

It can be applied to polymers in granular form or to any fabricated shape from which appropriate specimens can be cut.

In particular, this method consists of heating or cooling the material at a controlled rate in a specified purge gas at a controlled flow rate, then comparing the areas under the crystallization exotherm or fusion endotherm of the test material against the respective areas obtained by the similar treatment of a well-characterized standard.

Basically, DSC provides a rapid method for evaluating enthalpy changes accompanied by the first-order transitions of materials.

The heat of fusion, the heat of crystallization, and the effect of annealing may be generally evaluated in polymers that possess them. Differential scanning calorimetry may be used to assist in identifying specific polymers, blends, and certain polymer additives which exhibit thermal transitions.

This test method is useful for both process control and specification acceptance, as well for research purpose.

Results from DSC analysis performed on Z-ABS and Z-UltraT have been reported in terms of heat flow-temperature curves (Figure  and Figure ).

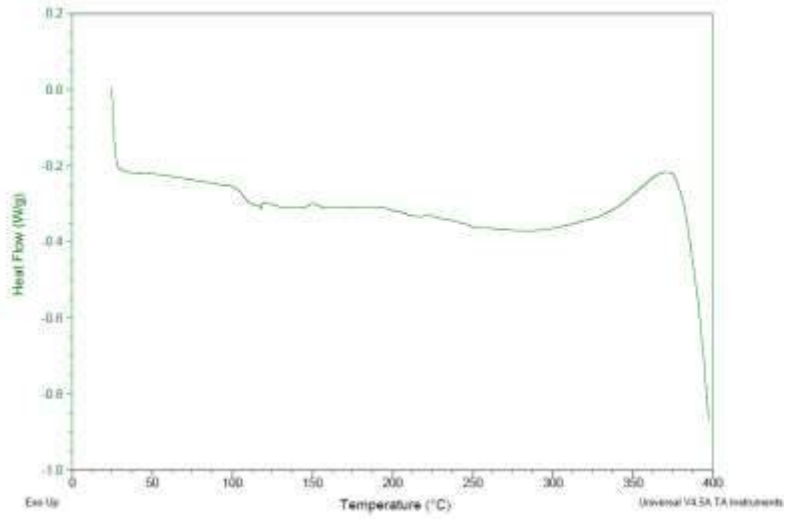


*Figure 2.1. Results obtained from DSC analysis: typical curve of heat flow versus temperature for Z-ABS.*

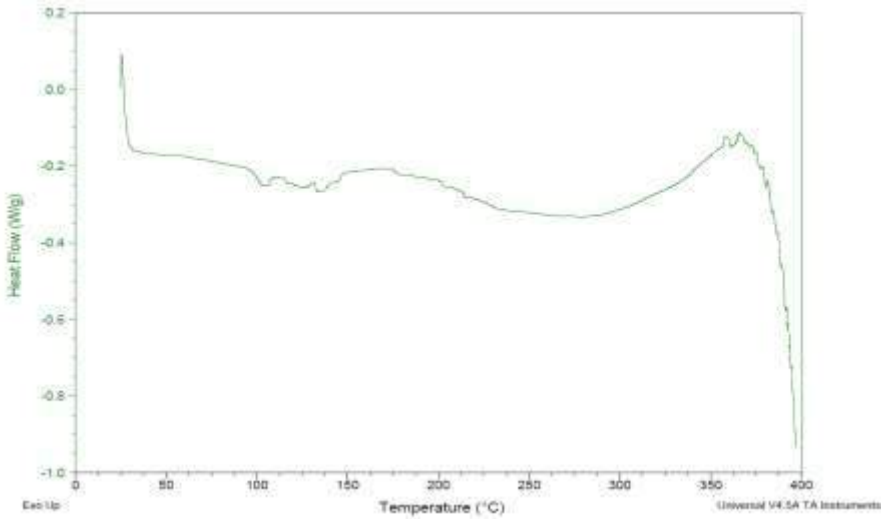


*Figure 2.2.  Results obtained from DSC analysis: typical curve of heat flow versus temperature for Z-UltraT*

Glass transition temperatures of about 125°C and 144°C were evaluated for Z-ABS and Z-UltraT, respectively.

On the other hand, thermogravimetric analysis (TGA) is a method of thermal analysis in which changes in chemical and physical properties of materials are evaluated as a function of increasing temperature at a constant heating rate, or as a function of time at a constant temperature and/or constant mass loss TGA may provide information about physical phenomena, such as second-order phase transitions, including absorption, adsorption, desorption, sublimation and vaporization.

TGA relies on a high degree of precision in three measurements: mass change, temperature, temperature change.

The basic instrumental requirements for TGA consist of a precision balance with a pan loaded with the sample, and a programmable furnace. The TGA apparatus continuously weighs a sample as it is heated to high temperatures.

As the temperature increases, several components of the sample can be decomposed. Thus, the weight percentage of each resulting mass change can be measured. Results are normally plotted with temperature on the X-axis and mass loss on the Y-axis.

The obtained results from TGA performed on Z-ABS and Z-UltraT have been reported in terms of weight-temperature curves (Figure and Figure 2.4).

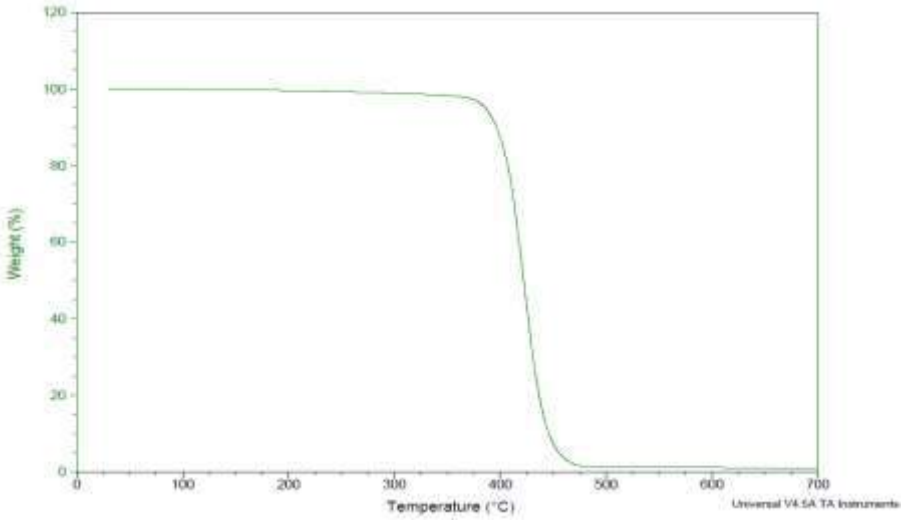


*Figure 2.3. Results obtained from TGA: typical weight versus temperature curve for Z-ABS*

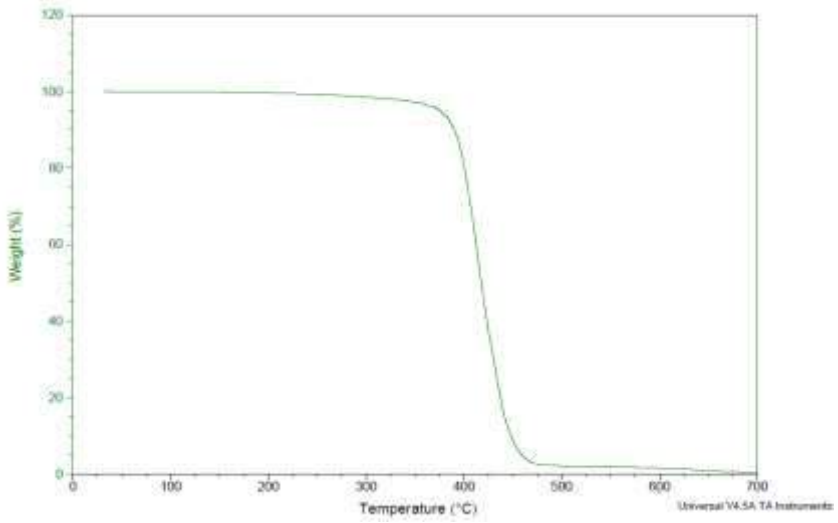


*Figure 2.4. Results obtained from TGA: typical weight versus temperature curve for Z-UltraT*

Results from TGA have allowed to assess the thermal stability of the materials.

Accordingly, in a specific temperature range, if a species is thermally stable, no mass change is observed.

Negligible mass loss corresponds to little or no slope in the TGA trace. TGA provides the upper use temperature of a material and beyond this temperature the material begins to degrade, thus providing interesting information in terms of process parameters.

## 2.3 Mechanical Analysis: Flexural Tests

Three-point bending tests were carried out on the different kinds of printed “building blocks” made of Z-ABS and UltraT, according to the ASTM D790 [51]. All the tests were performed using an IINSTRON 5566 testing machine. The support span-to-depth ratio was 16 to 1 (Figure Figure ).

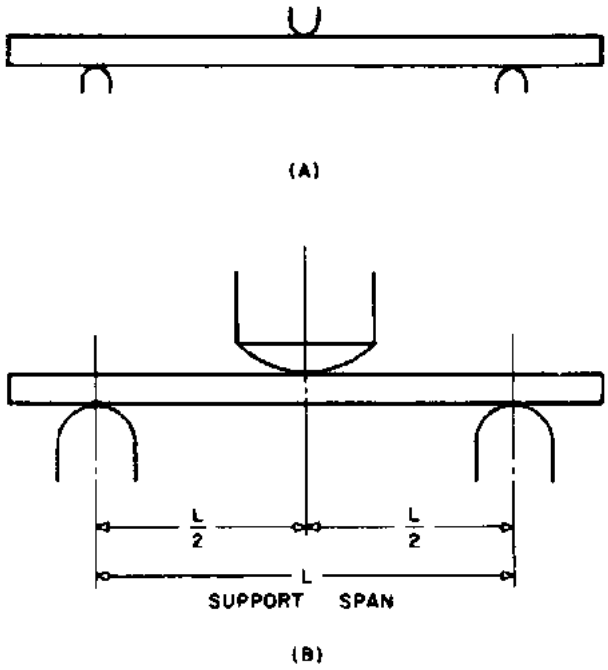


*Figure 2.5. Schematic representation of three-point bending tests*

Stress (σ) and strain (ε) were evaluated as follows:

$$\sigma = \frac{3FL}{2bd^2} \qquad (2.1)$$

$$\varepsilon = \frac{6D_f d}{L^2} \qquad (2.2)$$

where $D_f$ is the deflection of the specimen at the middle of the support span, F is the load at a given point of the load-deflection curve, L is the support span, b and d are the sample width and depth, respectively.

Typical stress-strain curves usually obtained from three-point bending tests was reported in Figure .

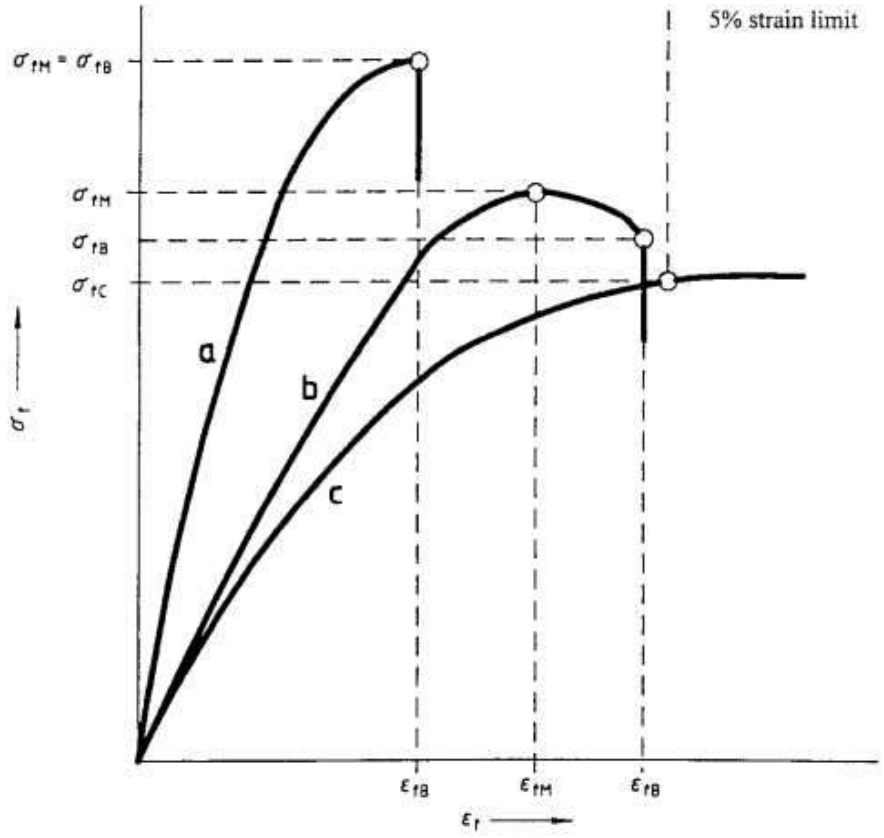


NOTE—Curve a: Specimen that breaks before yielding.
Curve b: Specimen that yields and then breaks before the 5 % strain limit.
Curve c: Specimen that neither yields nor breaks before the 5 % strain limit.

*Figure 2.6. Typical curves of flexural stress versus flexural strain obtained from three-point bending tests, according to the ASTM D790.*

Three-point bending tests on the two different kinds of printed "building blocks" made of Z-ABS and Z-UltraT evidenced similar stress-strain curves (Figure 2.7).

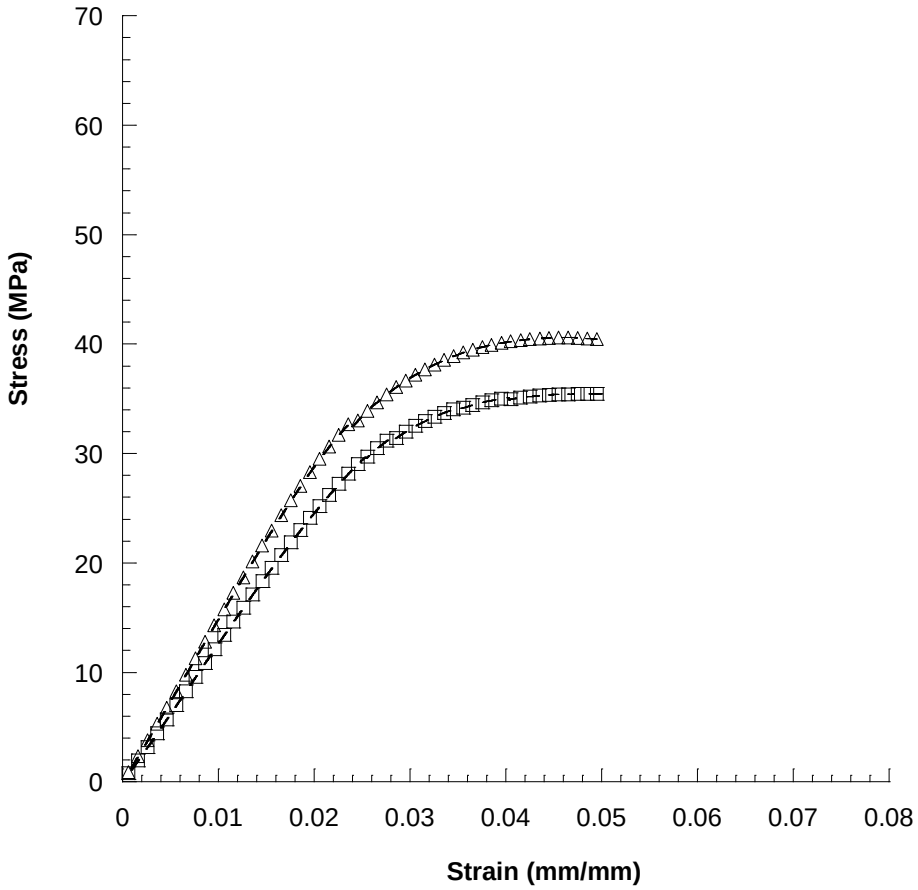


*Figure 2.7. Typical stress-strain curves obtained from three-point bending tests on the two different kinds of printed "building blocks" made of Z-ABS (□) and Z- UltraT (Δ).*

An initial linear region of the stress–strain curve was evident. Then, a decrease of the slope was observed.

Bending modulus (i.e., the slope of the linear region of the curve) and maximum stress were evaluated and reported as mean value ± standard deviation (

Table ).

| ***Sample*** | ***E (MPa)*** | $\sigma_{max} = \sigma_{fc}$ ***(MPa)*** |
|---|---|---|
| *Z - ABS* | *1211.1 ± 33.2* | *34.0 ± 0.3* |
| *Z - ULTRA T* | *1430.1 ± 31.9* | *40.1 ± 0.3* |

*Table 2.3. Results obtained from three-point bending: modulus (E) and maximum stress ($\sigma_{max}$) reported as mean value ± standard deviation.*

According to the ASTM D790, as all the specimens neither yields nor break before the 5% limit, $\sigma_{max}$ was equal to $\sigma_{fc}$ (flexural stress at 5 % strain limit).

As reported in

Table , Z-UltraT provided higher values of modulus and maximum stress than those obtained from Z-ABS.

# Chapter 3
# Design of 3D Virtual and Additive Manufactured Models

## 3.1 Design of 3D virtual and physical scale models of buildings

An additive manufactured physical model of a building (Chiesa di Santa Maria Francesca Saverio Cabrini – ex Padiglione della Civiltà Cristiana in Africa, Mostra d'Oltremare – Naples, Italy) was developed using the reverse engineering approach and the FDM technique. Different parts of the building were manufactured and then properly assembled.

The first step of the research was to review the most important characteristics of the buildings, the location, and an approach toward the methodology used to propose a reconstruction plan.

To design all the parts, a collection phase of high level data and images was made, taking into consideration the aspect of the state of the places, in many cases also focusing on the collection of texts, archives, etc. related to actual places.

For this reason, the information about the actual state of the sites was based on the possibility of using advanced techniques for image capture and analysis.

Staring from the current state of the building, a well-defined project was proposed.

Reverse engineering techniques (i.e., laser scanning, photogrammetry …) were used for the relief of the building, whereas FDM was employed to fabricate the parts of the building which were then properly assembled.

The case of the "Chiesa di Santa Maria Francesca Saverio Cabrini – ex Padiglione della Civiltà Cristiana in Africa, Mostra d'Oltremare – Naples, was taken into consideration especially due to the

complexity of the architectonic system, involving the use of both conventional and advanced technologies to obtain 3D relieves.

This approach represents an enormous potential of up-to-date, available and, above all, georeferenceble information, which is crucial for an architectural contextualized knowledge of the territory.

The acquisition of 3D data with laser scanner and/or photogrammetry generates a high resolution model. The same technique is used to detect both the architectonic compound of the above mentioned building and the surrounding environment.

The images were properly acquired and elaborated using different kinds of graphic softwares (i.e., Aigisoft Photoscan Professional, Geomagic…), thus all the models were further optimized.

The application of virtual 3D modelling allowed to a spatial analysis and verifications of the architectural features.

A specific methodology was considered during the whole design process of the built environment (i.e., building, interiors) using ArchiCAD 19, which is an architectural Building Information Model (BIM) CAD software for Macintosh and Windows developed by the Hungarian company Graphisoft. Such software offers computer aided solutions for handling all common aspects of aesthetics and engineering. In ArchiCAD 19, the application speed has been further enhanced by a technology innovation called "background processing," or more specifically, "predictive background processing."

Accordingly, several images of different perspective views were obtained (Figures 3.1 – 3.3).

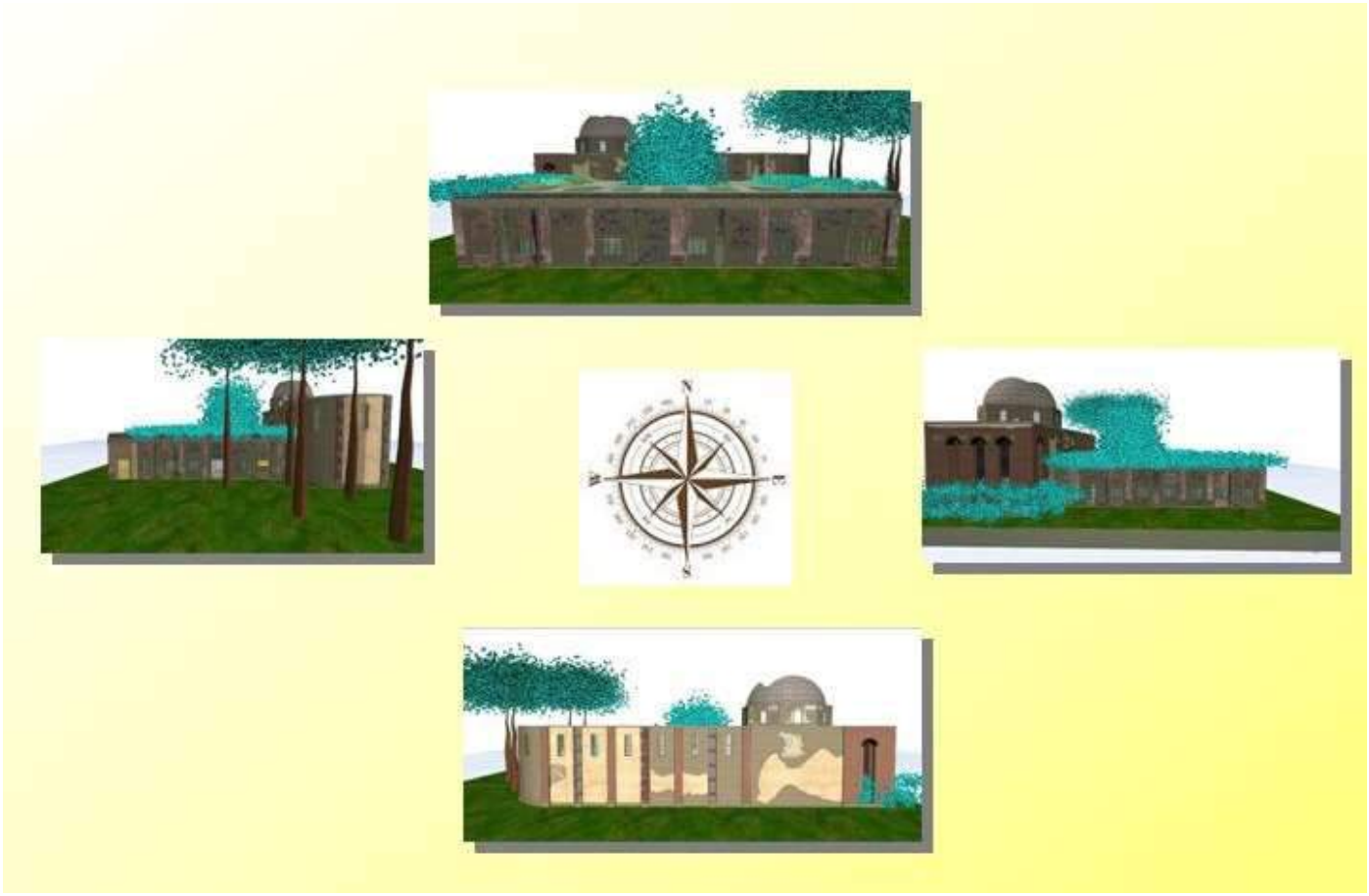

*Figure 3.1. Chiesa di Santa Maria Francesca Saverio Cabrini – ex Padiglione della Civiltà Cristiana in Africa, Mostra d'Oltremare – Naples, Italy: The current state - typical perspective views.*

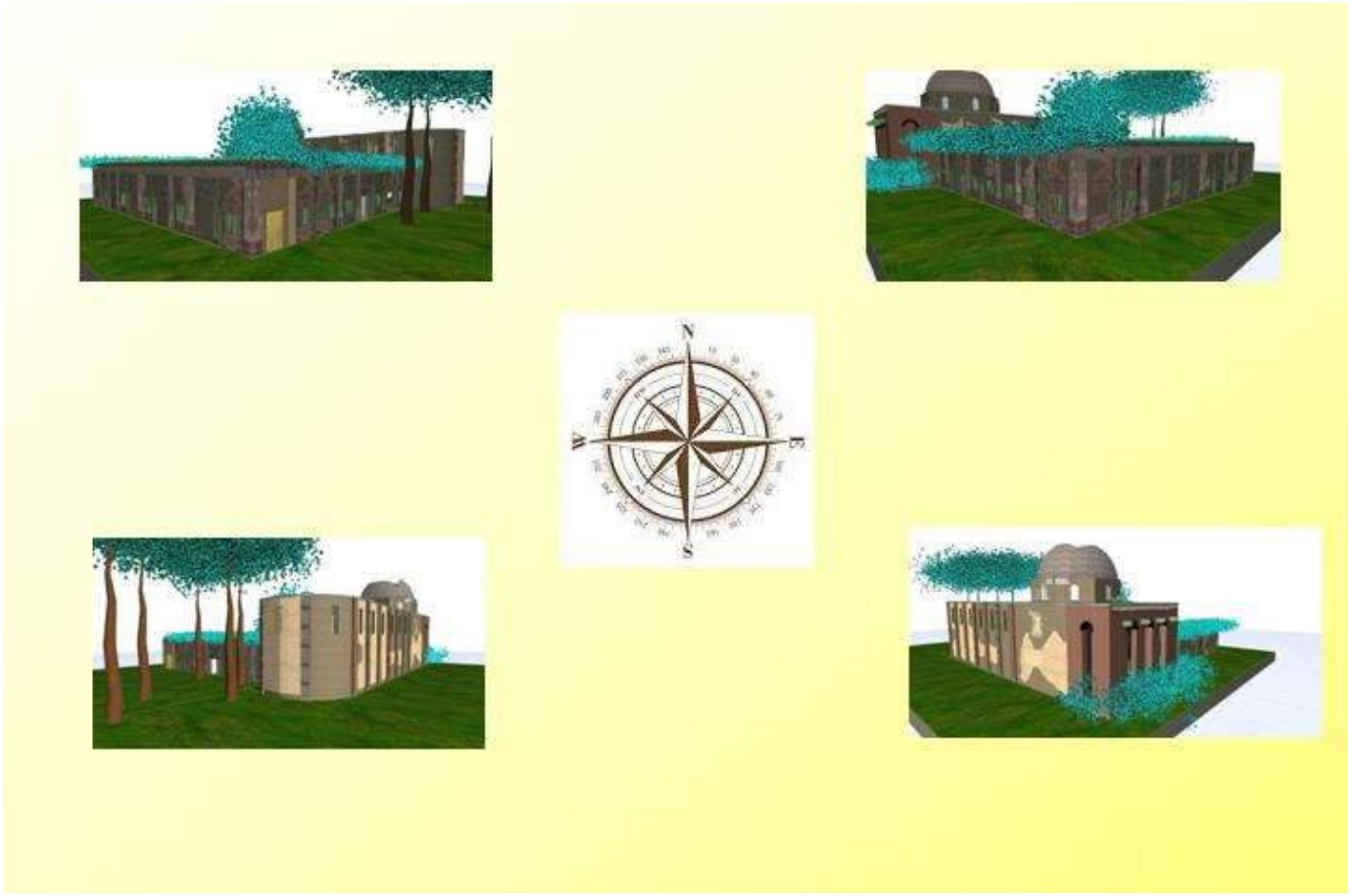


*Figure 3.2. Chiesa di Santa Maria Francesca Saverio Cabrini – ex Padiglione della Civiltà Cristiania in Africa, Mostra d'Oltremare – Naples, Italy: The current state - typical perspective views.*

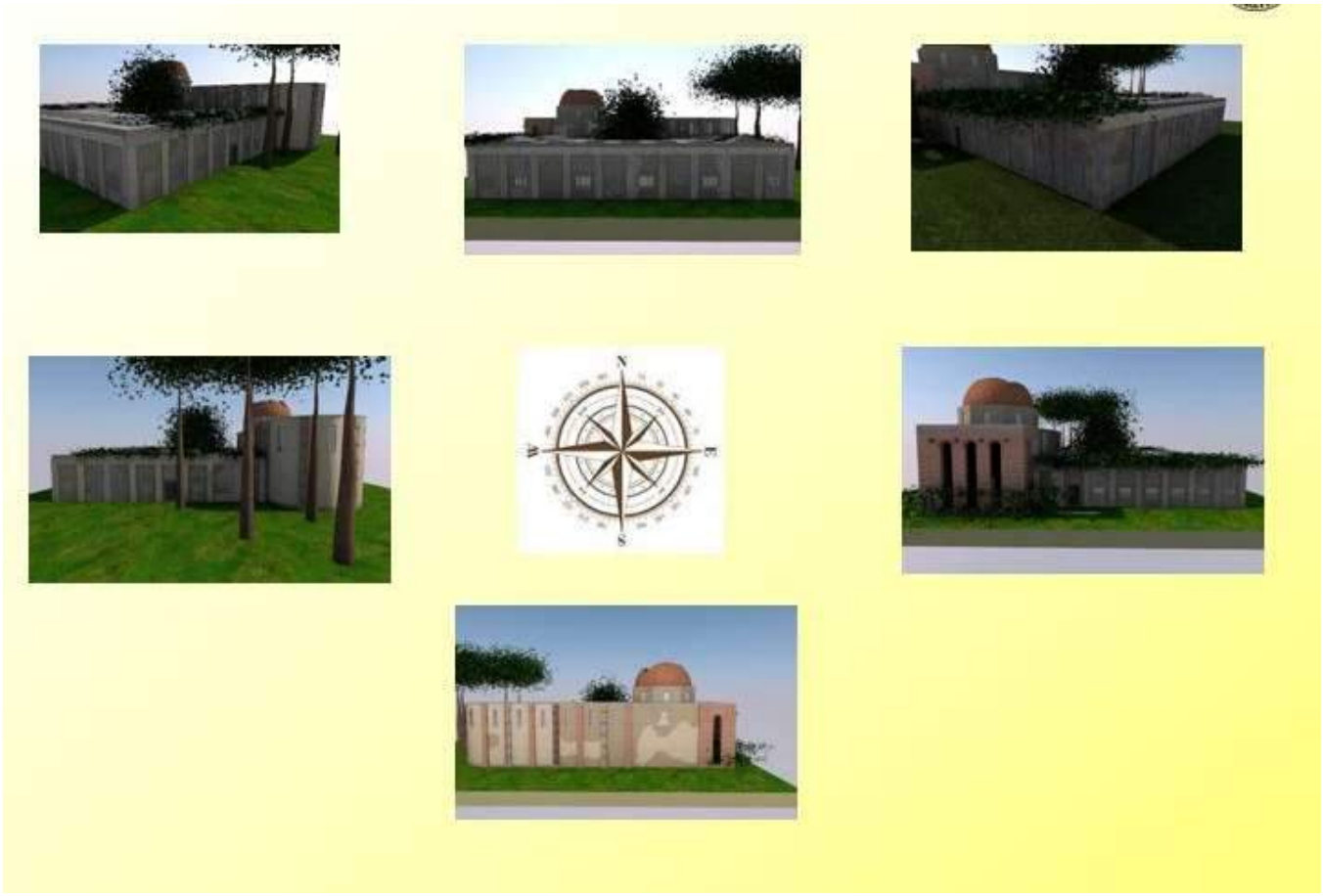

*Figure 3.3. Chiesa di Santa Maria Francesca Saverio Cabrini – ex Padiglione della Civiltà Cristiana in Africa, Mostra d'Oltremare – Naples, Italy: The current state - typical perspective views.*

As well reported, ArchiCAD also allowed to create a Virtual Building, a 3D Building Information Model (BIM) of an architectural design while simultaneously developing coordinated 2D construction documents.

In this context, 3D rendering is considered as a 3D computer graphics process of automatically converting 3D wire frame models into 2D images with 3D photorealistic effects or non-photorealistic rendering on a computer. Basically, rendering is the final process of creating the actual 2D image or animation from the prepared scene. However, over the past years different rendering methods have been developed.

In the current study, several design solutions were proposed for the building (Figure 3.4 ).

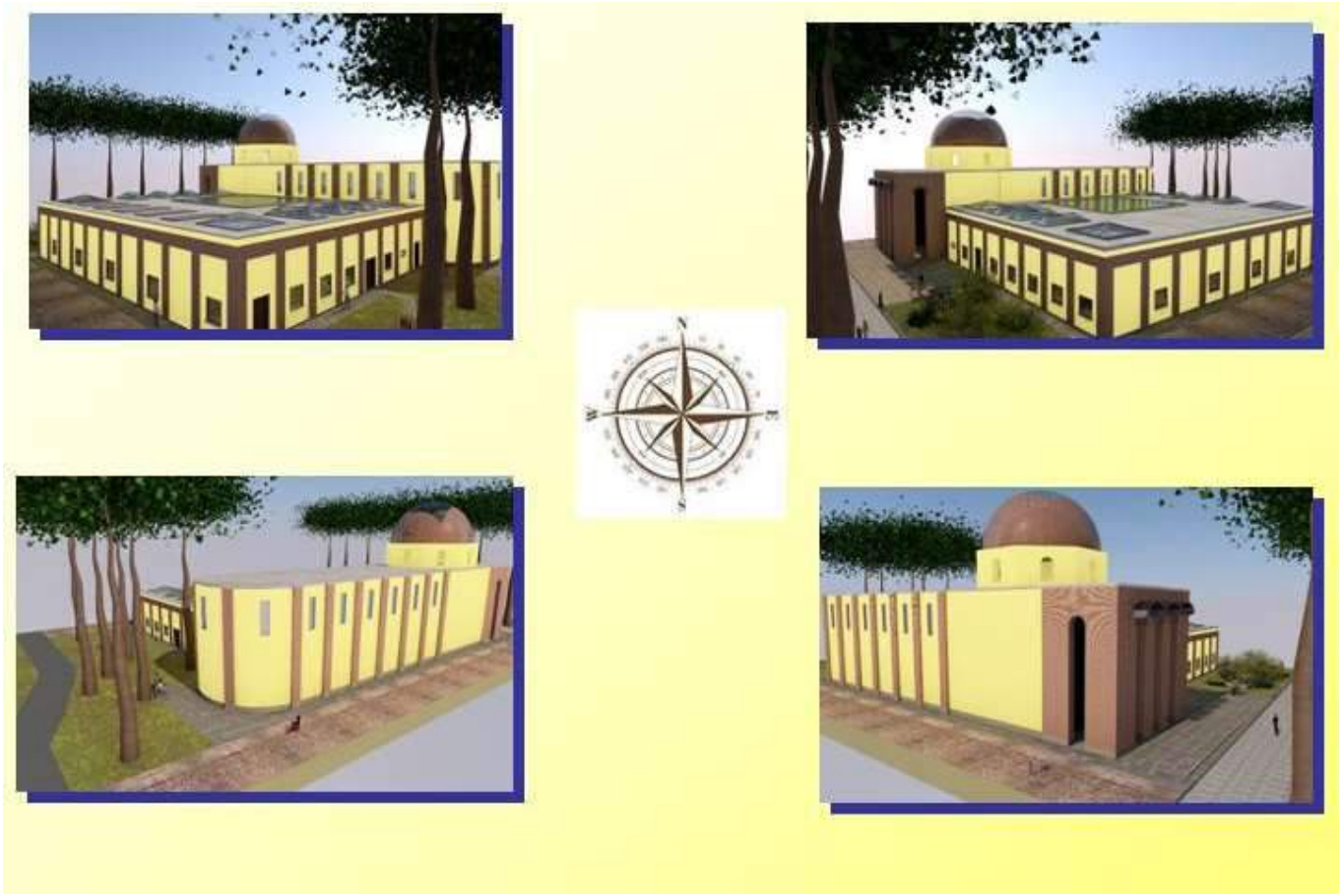

*Figure 3.4 Chiesa di Santa Maria Francesca Saverio Cabrini – ex Padiglione della Civiltà Cristiana in Africa, Mostra d'Oltremare – Naples, Italy: Design solutions - typical perspective views.*

Different potential solutions were also proposed for the novel interior design, taking into consideration several reconstructive hypotheses, which were based on specific constructive logics.

An interior design was proposed and organized in different spaces/rooms such as art gallery, conference room and relax space (Figures 3.5 – 3.7).

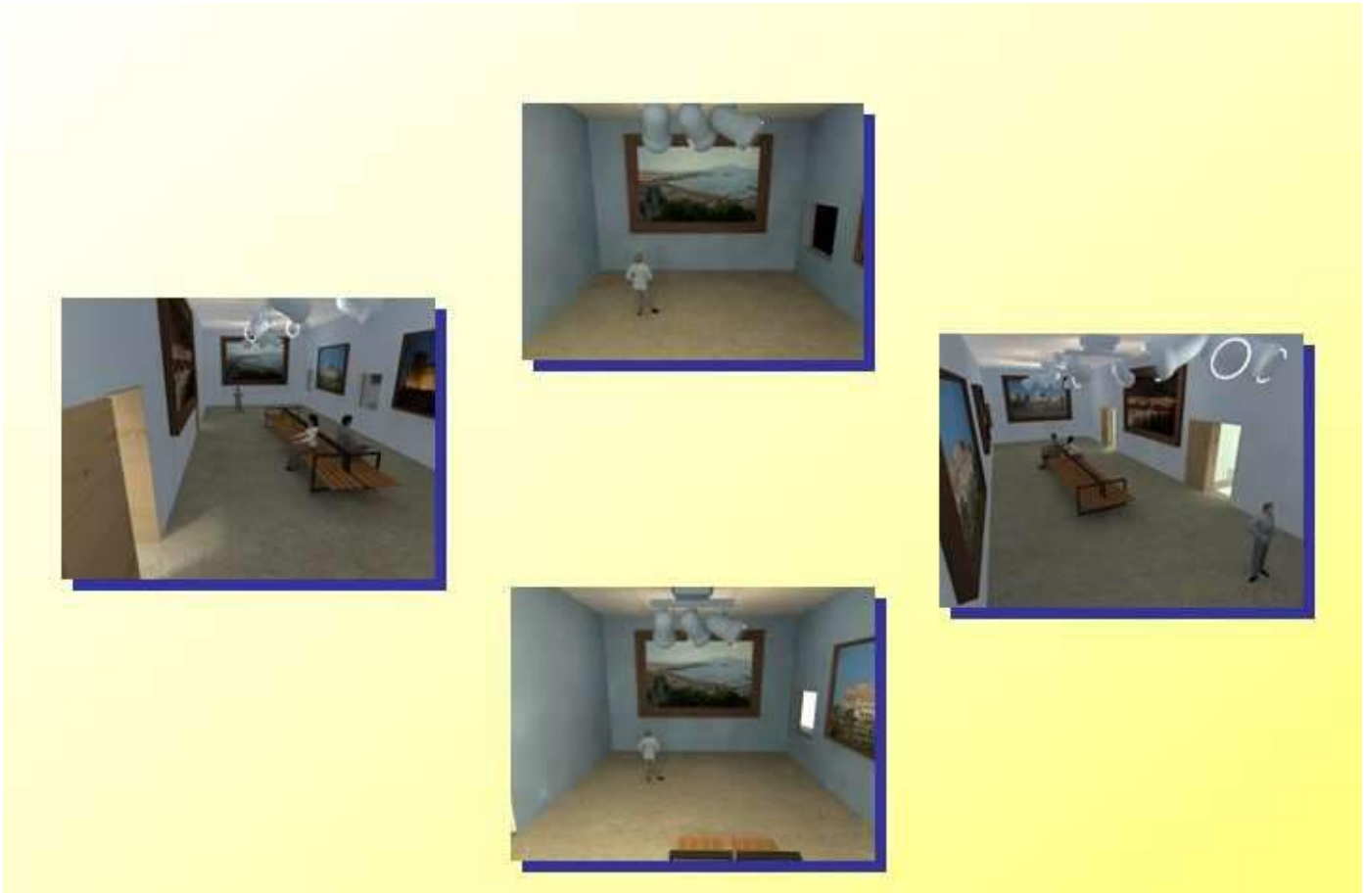

*Figure 3.5. Interior design: Art Gallery –elaboration steps.*

*Figure 3.6. Interior design: Conference room – final result.*

*Figure 3.7. Interior design: Relax Space.*

The ambient modelling was performed taking into account different parameters such as luminance levels and colour rendering index of the light source (Figure 3.8).

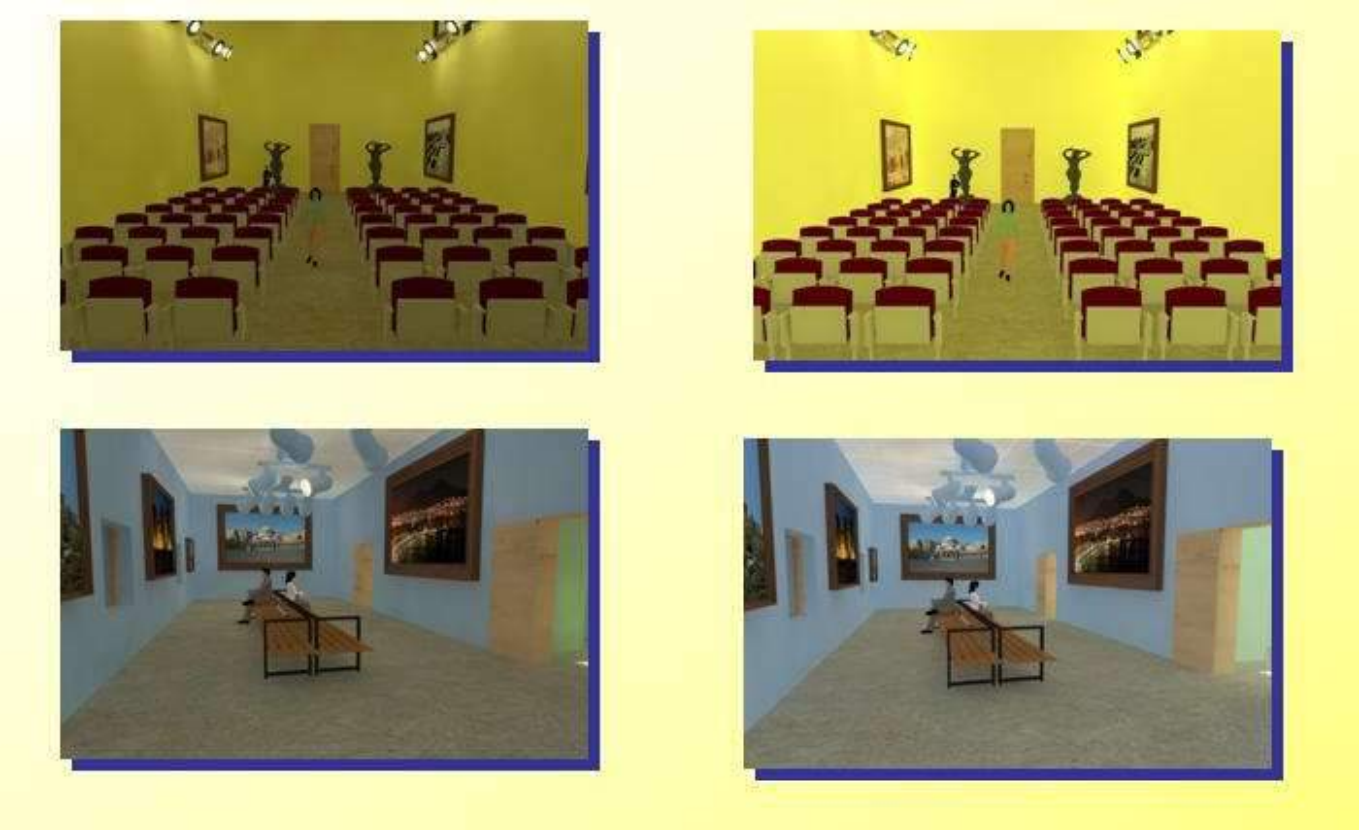

*Figure 3.8. Effects and comparisons using different parameters (i.e., luminance levels, colour rendering index of the light source…) - Congress Room and Art Gallery.*

Once all the features related to the virtual reconstruction of the external and interior parts of the building were optimized, the different part of the physical model were fabricated by FDM (Figure 3.9).

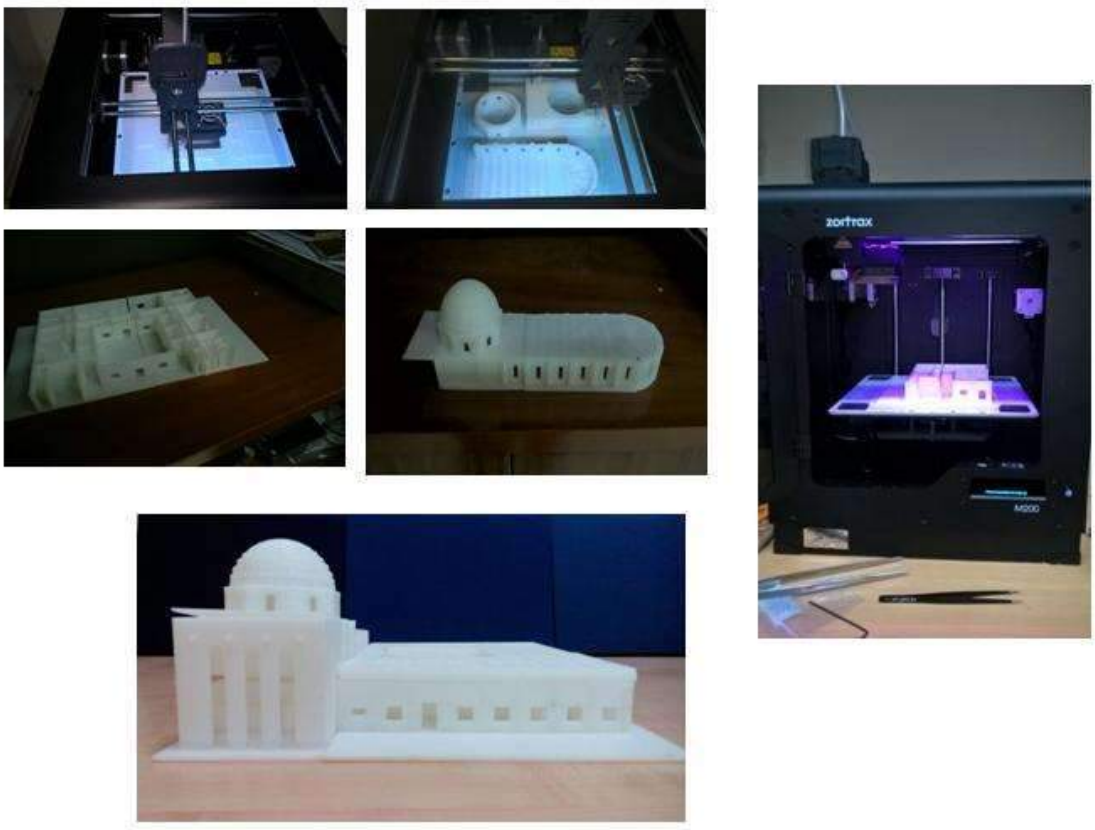


*Figure 3.9. Manufacturing process - different steps and results (i.e., apsis, atrium, dome, cloister…). Image of the assembled structure (Chiesa di Santa Maria Francesca Saverio Cabrini – ex Padiglione della Civiltà Cristiana in Africa, Mostra d'Oltremare – Naples, Italy).*

A schematic representation of the fabrication process is reported in figure 3.10.


*Figure 3.10. Design of a physical model of the building (Chiesa di Santa Maria Francesca Saverio Cabrini – ex Padiglione della Civiltà Cristiana in Africa, Mostra d'Oltremare – Naples, Italy) integrating image capture and analysis techniques with FDM.*

## 3.2 Development of 3D virtual and physical models – Artworks

Two bronze busts (two painters, Mariano Fortuny and Andrea Morelli - Zevallos Palace, Naples) were analyzed and manufactured by FDM using Z-ABS.

Benefiting from the image capture and analysis techniques though laser scanning and appropriate softwares, the exact shape/geometry and all the morphological features of the busts were reproduced (Figures 3.11-3.13) and 3D physical models were fabricated by FDM.

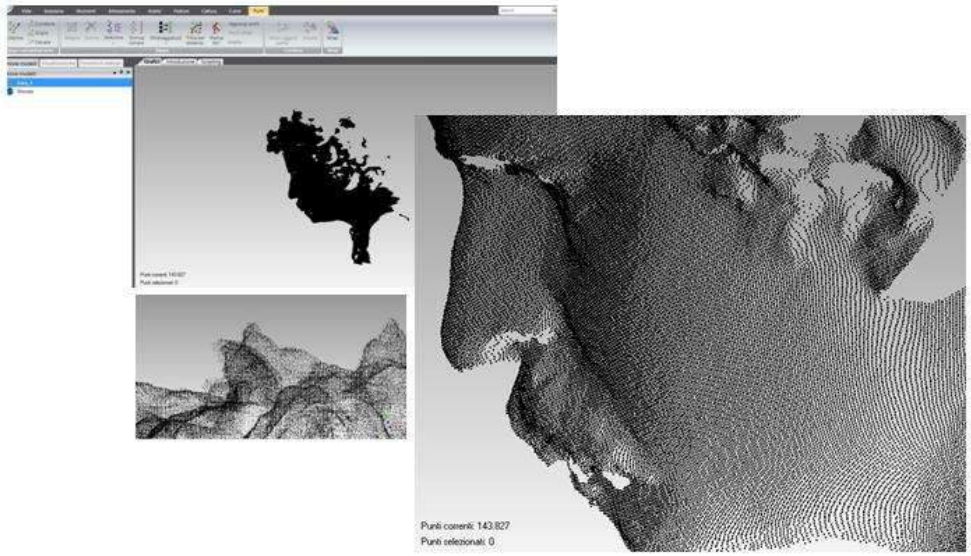


*Figure 3.11.Results from Laser scanning and cloud of points - Mariano Fortuny*

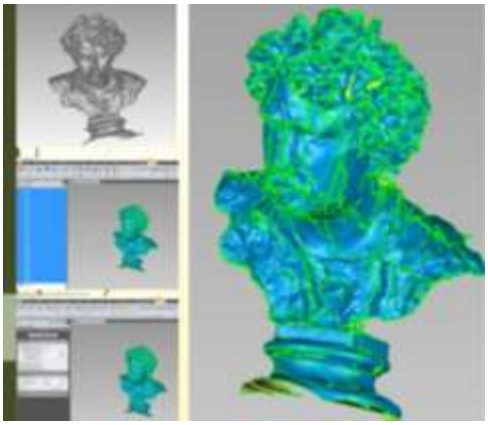

*Figure 3.12. Results from image capture and analysis techniques: different steps of 3D reconstruction - Mariano Fortuny*

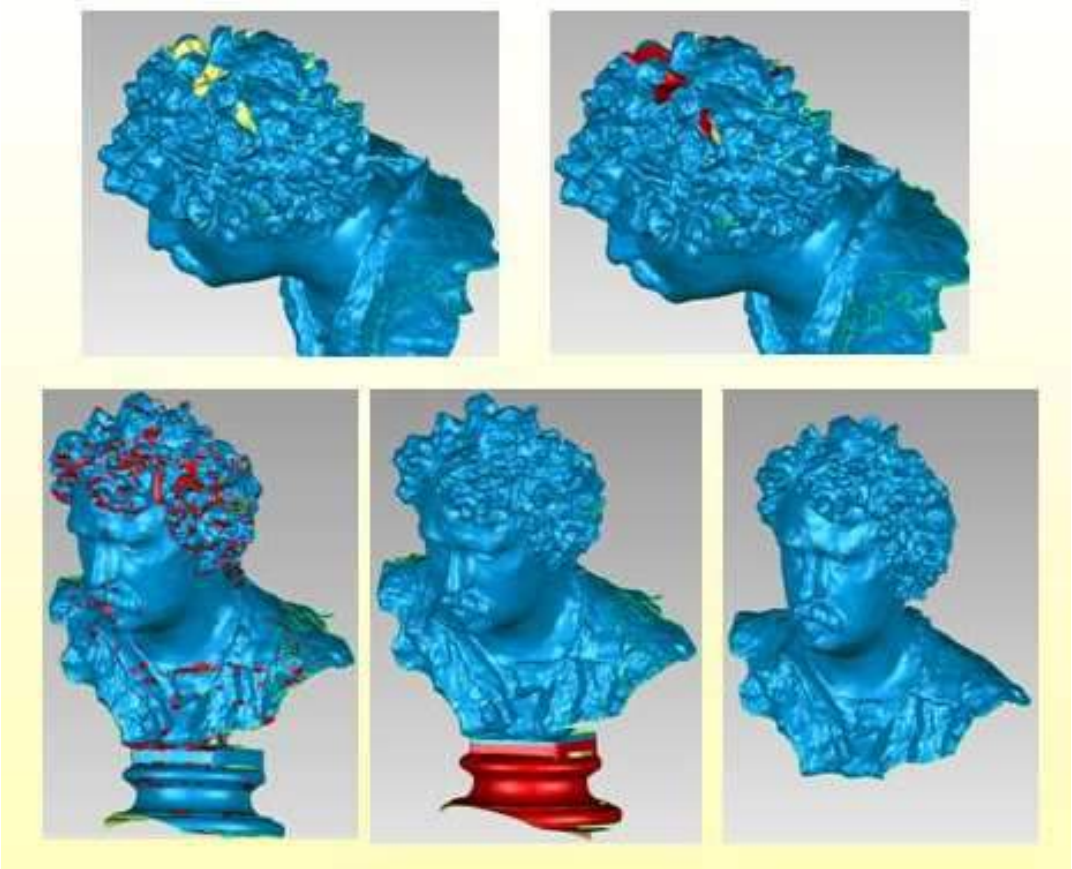

*Figure 3.13. Results from image capture and analysis techniques: different steps of 3D reconstruction - Mariano Fortuny.*

The 3D physical models of the bust was then fabricated by FDM (Figure 3.14), using a 3D printer (Zortrax S.A, Poland).

*Figure 3.14. Different steps in the design of a physical model of a bust (Mariano Fortuny) integrating image capture and analysis techniques with FDM.*

Taking into consideration the above reported approach, the other analyzed bronze bust (Domenico Morelli) was designed and manufactured (Figure 3.15).

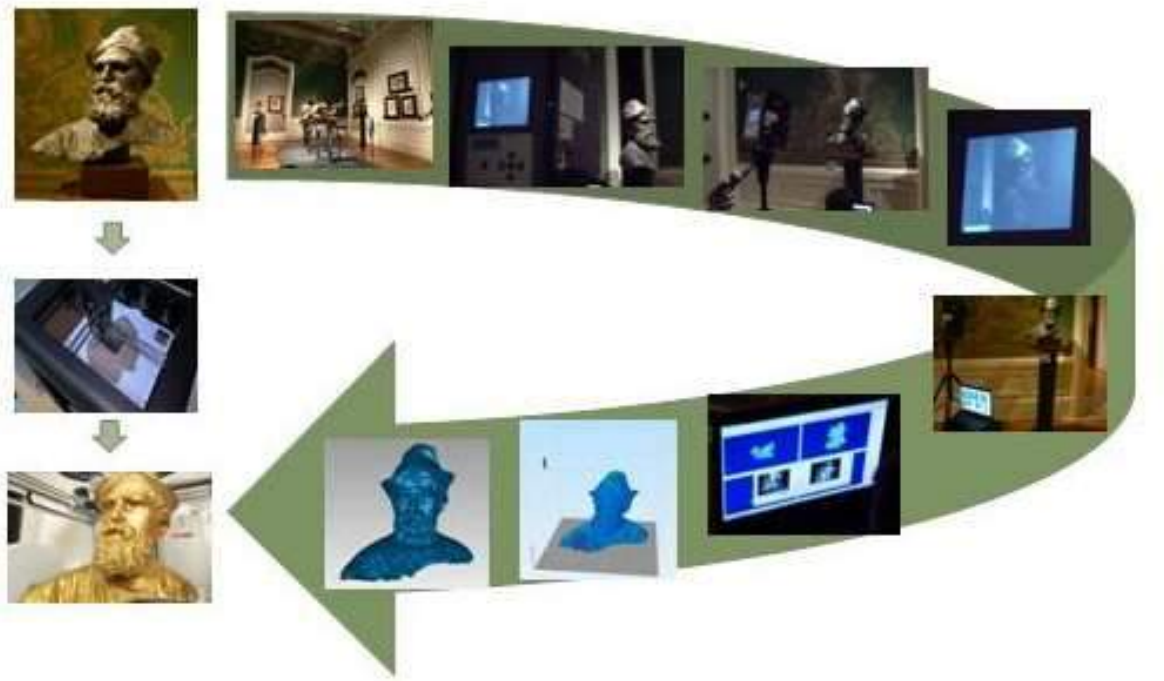

*Figure 3.15. Different steps in the design of a physical model of a bust (Domenico Morelli) integrating image capture and analysis techniques with FDM.*

## 3.3 Conclusions and future trends

Starting from a critical analysis of additive manufacturing technologies and materials, the current research evidenced the possibility to design 3D virtual and physical models for cultural heritage integrating the reverse engineering methods and tools with the additive manufacturing.

In particular, fused deposition modelling was considered as a versatile technology to design scale models of buildings and artworks.

Furthermore, the reported reverse engineering approach (i.e., laser scanning and photogrammetry) was also used for a church tabernacle (Chiesa dell'Annunziata – Marcianise, Caserta) (Figure 3.16).

*Figure 3.16. Tabernacle (Chiesa dell'Annunziata – Marcianise, Caserta): Images and preliminary results obtained from 3D reconstruction.*

The idea would be also to further optimize the image capture analysis techniques, comparing the results obtained from laser scanning and photogrammetry in terms of 3D reconstruction, as well as to develop an additive manufactured model of the tabernacle.

However, the proposed research would be considered as a first step of a future complex study towards the design of large-scale additive manufactured models for cultural heritage, also using multi-materials systems.

The research could be also related to a social impact project aiming at allowing blind persons "to build" a complete mental image of the reproduced structures.

# REFERENCES

[1] «ASTM F2792–10 Standard Terminology for Additive Manufacturing,» in *ASTM International Committee F42 on Additive Manufacturing*, ASTM, West Conshohocken, PA, 2009,.

[2] F. Pereira, F. Salvatore, F. Di Felice and M. Soave, "Experimental Investigation of a Cavitating Propeller in," in *Proc. of the Twenty-Fifth ONR Symposium on Naval Hydrodynamics*, St. John's, Newfoundland, Canada, 2004.

[3] F. Pereira, F. Salvatore and F. Di Felice, "Measurement and Modelling of Propeller Cavitation in Uniform," *J. of Fluids Engineering*, vol. 126, no. July, p. 671–679, 2004.

[4] S. F., "The INSEAN E779A Propeller Experimental," in *Tech. Rep. D4.1.3, INSEAN, VIRTUE WP4*, May, 2007.

[5] F. Salvatore, H. Streckwall and T. van Terwisga, "Propeller Cavitation Modelling by CFD - Results from," in *First International*, Trondheim, Norway,, June, 2009.

[6] ITTC, «Testing and extrapolation methods: propulsion, performance propulsion test,» in *Tech. Rep. 7.5-02-03-01.1*, International Towing Tank Conference, 2002.

[7] ITTC, «Testing and extrapolation methods: propulsion, Propulsion, Propulsor Open Water Test,» in *Tech. Rep. 7.5-02-03-02.1*, International Towing Tank Conference, 2002.

[8] I. Gibson, D. Rosen and B. Stucker, Additive Manufacturing Technologies, Springer Ed., 2010.

[9] A. Lanzotti, D. Del Giudice, A. Lepore, G. Staiano and M. Martorelli, "On the geometric accuracy of RepRap open-source three-dimensional printer," *Journal of Mechanical Design, Transactions of the ASME*, vol. 137, 2015.

[10] A. Lanzotti, M. Grasso, G. Staiano and M. Martorelli, "The impact of process parameters on mechanical properties of parts fabricated in PLA with an open-source 3-D printer," *Rapid Prototyping Journal*, vol. 21, 2015.

[11] A. Lanzotti, M. Martorelli and G. Staiano, "Understanding process parameter effects of reprap open-source three-dimensional printers through a design of experiments approach," *Journal of*

*Manufacturing Science and Engineering, Transactions of the ASME,* no. 137, 2015.

[12] W. E. Frazier, "Digital Manufacturing of Metallic Components: Vision," in *Solid Free Form Fabrication Proceedings*, Austin, TX, 2010.

[13] W. E. Frazier, "Metal Additive Manufacturing: A Review," *J. Mater. Eng. Perform.,* vol. 23, no. 6, p. 1917–1928, 2014.

[14] H. Ghariblu and S. Rahmati, "New Process and Machine for," *ASME J. Manuf. Sci. Eng.,,* vol. 136, no. 4, 2014.

[15] S. H. Huang, P. Liu, A. Mokasdar and L. and Hou, "Additive Manufacturing and Its Societal Impact: A Literature Review," *Int. J. Adv. Manuf. Technol.,,* vol. 67, no. (5-8), pp. 1191-1203, 2013.

[16] A. Council and M. Petch, "3D Printing: Rise of the Third Industrial Revolution," *Gyges 3D,,* p. 116, 2014.

[17] B. Berman, "3-D Printing: The New Industrial Revolution," *Bus. Horiz.,,* vol. 55, no. 2, pp. 155-162, 2012.

[18] 2. E. ISO/ASTM 52915, "Specification for Additive Manufacturing File Format (AMG) Version 1.1.".

[19] 2. E. ISO/ASTM 52921, «Terminology for Additive Manufacturing—Coordinate Systems and TestMethodologies.».

[20] R. Jones, P. S. E. Haufe, P. Iravani, V. Olliver, C. Palmer and B. A., "RepRap—The Replicating Rapid Prototyper," *Robotica,* vol. 29, no. 1, pp. 177-191, 2011.

[21] J. P. Kruth, "Material Increases Manufacturing by Rapid Prototyping," *CIRP Ann.*, vol. 40, no. 2, p. 1603–1615, 1991.

[22] G. Lart, "Comparison of Rapid Prototyping Systems," in *Proceedings of First European Conference on Rapid Prototyping*, University of Nottingham, Nottingham, UK,, 1992.

[23] N. R. Ippolito, Iuliano, L. and A. de Filippi, "A New User Part for Performance," in *Proceedings of Third European Conference on Rapid Prototyping and Manufacturing,,* University of Nottingham, Nottingham, UK, 1994.

[24] N. P. Juster and T. H. C. Childs, "“Linear and Geometric Accuracies From Layer Manufacturing,”," *CIRP Ann.*, vol. 43, no. 1, pp. 163-166, 1994.

[25] N. P. Juster and T. H. C. Childs, "A Comparison of Rapid Prototyping Processes," in *Proceedings of Third European Conference on Rapid Prototyping and Manufacturing*, University of Nottingham, Nottingham, UK, 1994.

[26] M. Shellabear, "Benchmarking Study of Accuracy and Surface Quality in RP Models," RAPTEC, Task 4.2, Report No. 2., 1999.

[27] M. Mahesh, Y. S. Wong, Fuh, Y. H. and H. T. Loh, "Benchmarking for Comparative Evaluation of RP Systems and Processes," *Rapid Prototyping J.*, vol. 10, no. 2, pp. 123-135, 2004.

[28] T. B. Sercombe and N. Hopkinson, "Process Shrinkage and Accuracy During Indirect Laser Sintering of Aluminum," *Adv. Eng. Mater.*,, vol. 8, no. 4, pp. 260-264, 2006.

[29] M. Fahad and N. Hopkinson, "A New Benchmarking Part for Evaluating the Accuracy and Repeatability of Additive Manufacturing (AM) Processes," in *2nd International Conference on Mechanical, Production and Automobile Engineering (ICMPAE 2012)*, Singapore, 2012.

[30] P. F. Jacobs, "Rapid Prototyping & Manufacturing: Fundamentals of StereoLithography," *Society of Manufacturing Engineers (SME), Dearborn, MI*, p. 434, 1992.

[31] P. F. Jacobs, "StereoLithography and other RP&M Technologies: from Rapid Prototyping to Rapid Tooling," *Society of Manufacturing Engineers (SME), Dearborn, MI*, p. 450, 1996.

[32] S. H. Park, "Robust Design and Analysis for Quality Engineering," London, UK, Chapman & Hall, 1996.

[33] M. D. C., "Design and Analysis of Experiments 5 th edition," Wiley, 1997.

[34] D. Montgomery, P. E. and V. G., in *Engineering statistic 5th ediion*, Wiley & Sons, 2011.

[35] P. J. Besl and N. D. McKay, "A Method for Registration of 3-D Shapes," *IEEE Trans. Pattern Anal. Mach. Intell.*, vol. 14, no. 2, pp. 239-256, 1992.

[36] K. M.W., J. Fuh and L. Lu, "Direct Metal Laser Sintering for rapid tooling: processing and characterization of EOS parts," *Journal of Materials Processing Technology*, 2001.

[37] S. J. A., "Materials standards for Additive Manufacturing," in *NIST – Workshop*, 2013.

[38] A. Simchi, F. Petzoldt and H. and Pohl, "On the Development of Direct Metal Laser Sintering for Rapid Tooling," *J. Mater. Process. Technol,* vol. 141, no. 3, pp. 319-328, 2003.

[39] M. W. Khaing, J. Y. H. Fuh and L. Lu, "Direct Metal Laser Sintering," *J. Mater.*, vol. 113, no. 1-3, pp. 269-272, 2001.

[40] K. Senthilkumaran, P. M. Pandey and P. V. M. Rao, "Influence of Building Strategies on the Accuracy of Parts in Selective Laser Sintering," *Mater. Des.*, vol. 30, no. 8, pp. 2946-2954, 2009.

[41] Y.-A. Song and W. Koenig, "Experimental Study of the Basic Process Mechanism for Direct Selective Laser Sintering of Low-Melting Metallic Powder," *CIRP Ann. Manuf. Technol.*, vol. 46, no. 1, pp. 127-130, 1997.

[42] J. Delgado, J. Ciurana and C. A. Rodrıguez, "Influence of Process Parameters on Part Quality and Mechanical Properties for DMLS and SLM With ron-BasedMaterials," *Int. J. Adv. Manuf. Technol.,* vol. 60, no. 5-8, pp. 601-610, 2012.

[43] M. Wong, I. Owen, C. J. Sutcliffe and A. and Puri, "Convective Heat Transfer and Pressure Losses Across Novel Heat Sinks Fabricated by Selective Laser Melting," *Int. J. Heat Mass Transfer,* vol. 52, no. 1-2, pp. 281-288, 2009.

[44] F. Calignano, D. Manfredi, E. P. Ambrosio, L. Iuliano and P. Fino, "Influence of Process Parameters on Surface Roughness of Aluminum Parts Produced by DMLS,"," *Int. J. Adv. Manuf. Technol.,* vol. 67, no. 9-12, pp. 2743-2751, 2013.

[45] N. Read, W. Wang, K. Essa and M. Attallah, "Selective laser melting of AlSi10Mg: Process optimisation and mechanical properties development," *Materials & Design,* vol. 65, pp. 417-424, 2015.

[46] G. Staiano, A. Gloria, M. Martorelli, A. Lanzotti and C. Pensa, "Experimental Study of Naval Propellers Hydrodynamic Performances to Adopt New Additive Manufacturing Processes," in *Virtual Concept International Workshop on Major Trends in Product Design*, Bordeaux (France, 2016.

[47] Zortrax, «Material Data Sheet: Z-ABS».

[48] Zortrax, «Material Data Sheet: Z-UltraT».

[49] ASTM-D3417, "Standard Test Method for Enthalpies of Fusion and Crystallization of Polymers by Differential Scanning Calorimetry (DSC)," ASTM International, West Conshohocken, PA, 1999.

[50] ASTM-D3418, "Standard Test Method for Transition Temperatures and Enthalpies of Fusion and Crystallization of Polymers by Differential Scanning Calorimetry," ASTM International, West Conshohocken, PA,, 2015.

[51] ASTM-D790, "Standard Test Methods for Flexural Properties of Unreinforced and Reinforced Plastics and Electrical Insulating Materials," ASTM International, West Conshohocken, PA, 2002.

- PhD Thesis:
  Staiano Gabriele, 2016. "**Hydrodynamic performance of additive manufacturing marine propellers"**, **PhD program in "Ingegneria Aerospaziale, Navale e della Qualità",** 28th Cycle.